Four discrete positions electromagnetic actuator: modelling and experimentation

Laurent Petit, Christine Prelle, Emmanuel Dore, Frédéric Lamarque, Maxence Bigerelle

Four discrete positions electromagnetic actuator: modelling and experimentation

Laurent Petit, Christine Prelle, Emmanuel Doré, Frédéric Lamarque, Maxence Bigerelle

Abstract—**In this article, an electromagnetic actuator having four discrete positions is discussed. The principle, the modelling and an experimental device of this actuator are presented in this study. This actuator is composed of a mobile permanent magnet, four fixed permanent magnets, which ensure the holding of the discrete positions, and two perpendicular wires to switch independently in two perpendicular directions. The mobile part has four discrete positions, two in each direction. An electromagnetic actuator modelling has been realized to compute the magnetic and electromagnetic forces exerted on the mobile magnet and its displacement. The experimental device was designed using this model and then manufactured. The stroke of the mobile part is 1 × 1 mm. The driving current ranges from 3 A to 7 A. A comparison between experimental and modelled results is carried out. A good agreement on the displacement curves and on the rise times are observed for all the range of controlling currents.**

Index Terms—**Actuators, Digital mechanisms, Electromagnetic devices**

I. Introduction

In the literature, a numerous electromagnetic actuators is described, studied and used. These actuators can be classified into two categories among their way to create the displacement, the analogical and the digital actuators. The main characteristic of the analogical actuators is that they can theoretically reach any position between the extreme positions of the stroke. Numerous architectures and types of actuators with dedicated control law exist. For example, multi degree of freedom actuator [1], [2], linear actuator [3], [4], rotary actuator [5] and spherical actuator [6], [7] can be found in the literature.

On the contrary, the actuators based on the digital principle possess only few discrete positions and can not reach intermediate positions. However, these actuators have two main advantages for displacement generation in comparison with the analogical actuators. The first one is the low energy consumption such that energy supply is only needed to switch between the discrete positions. Pulsed signals used to generate the displacement allow reaching higher current value in electrical wires than continuous current [8] and lowers the undesirable effects like Joule effect. The second advantage is an open loop binary control. Indeed, a digital actuator ensures highly repeatable and accurate positions at the ends of the stroke which can lead to a sensor-less design simplifying the electrical connection and the integration of the actuator in meso or micro-mechanical systems. The limited stroke represents the main drawback of the digital actuation. However, an assembly of several digital actuators can permit a variable stroke.

The digital principle is used in several applications where a mobile part is displaced between two discrete positions. The main application is optical [9], electrical [10] or fluidic [11], [12] switches. The mobile part is displaced between the open (ON) and closed (OFF) positions. Moreover, digital actuators can also be assembled in parallel to compose a tactile display [13] or in serial to compose a binary modular robot [14].

Bistable actuators are particular digital actuators possessing a supplementary advantage: they remain at one of their local minimum states without energy input [15]. This effect ensures the bistability of positioning then the holding of the stable positions. In a simple digital actuator, a holding of the discrete positions can be added to maintain and to improve the positioning of the mobile part in discrete positions. Some analogical actuators have also the ability to maintain their position after a displacement [16]-[19] means of by maintaining the driving current. When this current is cut off, they remain in the central stable position.

To realize a digital actuator, various physical principles are used [9]-[13], [20]-[24]. Electromagnetic actuation is well adapted because the holding effect could be easily obtained magnetically with Permanent Magnets (PMs).

In this work, an electromagnetic actuator based on the digital principle is presented. Compared with those in the literature, it has the particularity of performing displacements in two perpendicular directions. It is not composed of an assembly of two perpendicular digital actuators but only one which has four discrete positions, two in each direction. The advantages of this structure are the compactness of the device and the reduction of the assembly errors. In this paper, the principle of the actuator and a modelling are presented. This modelling is used to design the experimental device which is manufactured. Finally, a comparison between experimental and modelling results are carried out.

Manuscript received October 3, 2008.

L. Petit, C. Prelle, E. Doré, F. Lamarque and M. Bigerelle members of the Roberval Laboratory, University of Technology of Compiègne (UTC), Rue du Docteur Schweitzer, 60203 Compiègne cedex, France. (+33 (0) 3 44 23 44 23, fax: +33 (0) 3 44 23 52 29; e-mail: laurent.petit@utc.fr, christine.prelle@utc.fr, emmanuel.dore@utc.fr, frederic.lamarque@utc.fr, maxence.bigerelle@utc.fr).

II. PRINCIPLE

The mobile part of the digital actuator is composed of a square Mobile Permanent Magnet (MPM) which can reach four discrete positions. The holding effect is generated magnetically with four Fixed Permanent Magnets (FPMs) placed at each side of the MPM (Fig. 1). The FPMs exert a magnetic attraction force on the MPM when it is near them. Two perpendicular wires placed below the MPM are used to produce the driving force. When a current passes through a wire, an electromagnetic force (or Lorentz force) appears because of the presence of the flux density from the MPM. Unlike the holding force which is always active, the driving force is only active during the transition of the MPM between two discrete positions. The displacement direction is perpendicular to the wire axis and is limited by two stops in each direction. To study the actuator, a coordinates system is defined (Fig. 1). Its origin is located in the middle of the square stop (Fig. 1a) and at 1 mm above the plane on which the MPM slides (Fig. 1b). The device has two independent displacement axes (x-axis and y-axis) and four discrete positions.

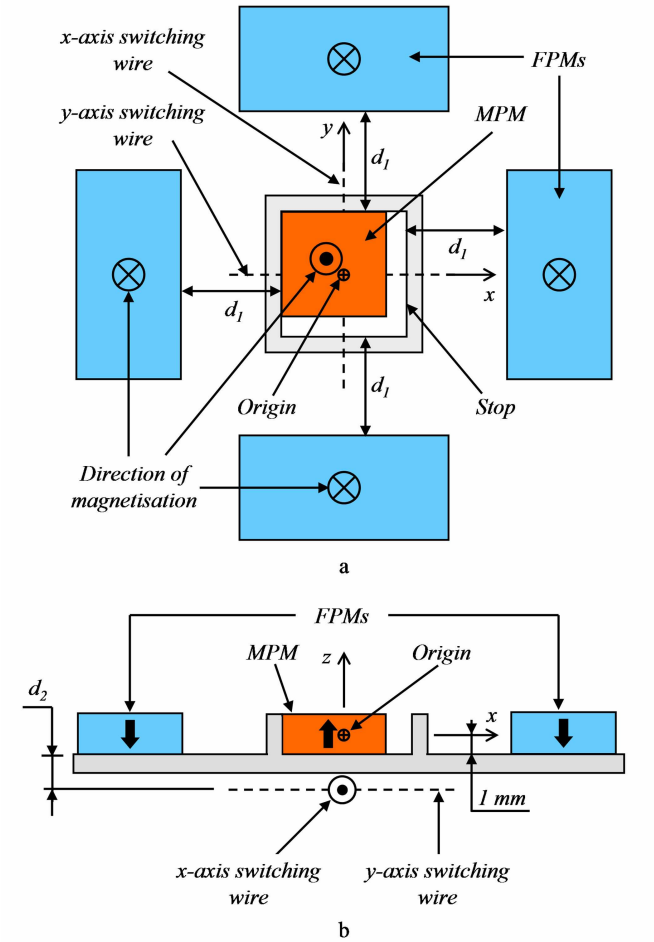

Fig. 1. Principle of the four discrete positions actuator
a. Side view b. Top view

When the MPM is in the position (–x ; +y) (Fig. 1) and if a current passes through the y-axis wire (called "x-axis switching wire") in the –y-direction, a Lorentz force is exerted on the wire in the –x-direction because the flux density is oriented in the +z-direction. The direction of the force acting on the wire is obtained by the left hand rule. The wire is fixed then an opposite force is exerted on the MPM which switches in the +x-direction and reaches the position (+x ; +y). During the switch, if a second current passes through the x-axis wire (called "y-axis switching wire") in the +x-direction, a Lorentz force is exerted on the wire in the –y-direction then an opposite force is exerted on the MPM in the +y-direction. This force increases the holding effect which can be interesting to minimize the straightness errors. In that case, the y-axis wire is called "driving wire" and the x-axis wire "holding wire".

III. MODELLING

To design the actuator, a modelling is realized. The first objective of this one is to compute the different forces exerted on the MPM. This computation has been used to design the experimental device. The second objective is to compute the displacement between two discrete positions depending on the controlling currents in order to correlate the simulated results with the experimental results.

To compute the electromagnetic and the magnetic forces, the flux density generated by a Permanent Magnet (PM) must be first modelled. In the next paragraphs, an analytical modelling of flux density is presented and two models of the magnetic and electromagnetic forces are realized using this analytical flux density modelling.

A. Analytical flux density modelling

The analytical flux density modelling is based on the charge model. Using this model, a PM is reduced to a distribution of equivalent magnetic charge. To realize this analytical modelling, we suppose that each PM is rectangular, in free space, its geometry is considered perfect and its magnetization is considered uniform and oriented along the z-axis.

The expressions of the three components of the flux density (B_x, B_y, B_z) for any point in the space (x, y, z) are given in Equations (1) [25]. The values ($x_2 - x_1$, $y_2 - y_1$, $z_2 - z_1$) correspond to the dimensions of the PM.

B. Force between two PMs

The second step is to model the magnetic force exerted between two PMs. Two PMs (PM1 and PM2) are considered fixed and their elastic deformation is neglected. Their magnetizations are considered uniform and orientated along z-axis. The expression of the force exerted by PM2 on PM1 is given in Equation (2) [25].

The σ_m represents the surface charge density of the two surfaces S where the poles of PM1 are located. The $\mathbf{B}_{ext}$ vector is the flux density generated by PM2 around PM1 and is computed with Equations (1). Because in most cases it is not possible to evaluate Equation (2) analytically, the force is obtained by discretizing the surfaces S of PM1 in p surfaces ΔA_p. The flux density is computed for each ΔA_p surface and the force is obtained with Equation (3) [25].

$$B_x(x,y,z)=\frac{\mu_0 M}{4\pi}\sum_{k=1}^{2}\sum_{m=1}^{2}(-1)^{k+m}\ln\left(F(x,y,z,x_m,y_1,y_2,z_k)\right)$$
$$B_y(x,y,z)=\frac{\mu_0 M}{4\pi}\sum_{k=1}^{2}\sum_{m=1}^{2}(-1)^{k+m}\ln\left(H(x,y,z,x_1,x_2,y_m,z_k)\right) \quad (1)$$
$$B_z(x,y,z)=\frac{\mu_0 M}{4\pi}\sum_{k=1}^{2}\sum_{n=1}^{2}\sum_{m=1}^{2}(-1)^{k+n+m}\times\tan^{-1}\left(\frac{(x-x_n)(y-y_m)}{(z-z_k)}\,g(x,y,z;x_n,y_m,z_k)\right)$$

$$F(x,y,z,x_m,y_1,y_2,z_k)=\frac{(y-y_1)+\left[(x-x_m)^2+(y-y_1)^2+(z-z_k)^2\right]^{1/2}}{(y-y_2)+\left[(x-x_m)^2+(y-y_2)^2+(z-z_k)^2\right]^{1/2}}$$
$$H(x,y,z,x_1,x_2,y_m,z_k)=\frac{(x-x_1)+\left[(x-x_1)^2+(y-y_m)^2+(z-z_k)^2\right]^{1/2}}{(x-x_2)+\left[(x-x_2)^2+(y-y_m)^2+(z-z_k)^2\right]^{1/2}}$$
$$g(x,y,z;x_n,y_m,z_k)=\frac{1}{\left[(x-x_n)^2+(y-y_m)^2+(z-z_k)^2\right]^{1/2}}$$

$$\mathbf{F}_{Magnetic}=\oint_S \sigma_m \mathbf{B}_{ext}\,ds \quad (2)$$

$$\mathbf{F}_{Magnetic}=\sum_p \sigma_m(x_p)\mathbf{B}_{ext}(x_p)\Delta A_p \quad (3)$$

C. Force between PM and wire

The third step is the modelling of the electromagnetic force exerted on a PM by a wire surrounded by the external flux density ($\mathbf{B}_{ext}$) generated by the PM. The expression of this Lorentz force acting on the wire when a current (I) passes through it is given in Equation (4) [25]. Equations (1) are used to compute the flux density generated by the PM around the wire.

$$\mathbf{F}_{Electromagnetic}=I\int_{wire} d\mathbf{l}\times\mathbf{B}_{ext} \quad (4)$$

Moreover, computations of the magnetic field generated by the current in the wires have been realized with a semi-analytical software (RADIA) which shows that the influence of this effect represents 0.3% of the total force exerted on the MPM. As a consequence, in this modelling, the magnetic field generated by the current in the wires is then not considered because it is negligible in comparison with the magnetic effect between the MPM and the FPMs and the electromagnetic effect between the MPM and the wires.

D. Design of the device

The three models (flux density, magnetic and electromagnetic forces) were compared with semi-analytical and FEM models which permit to validate them. The presented models were then used to design the digital actuator. The interactions between the MPM, the four FPMs and the two wires were considered. The flux density exerted around the MPM ($\mathbf{B}_{ext}$) is the sum of the contribution of each FPM and the total force exerted on the MPM is the sum of the magnetic and electromagnetic forces.

The properties of the NdFeB PMs which compose the experimental device are given in Table I. In a first study, several computations of forces were realized and we have estimated that under normal conditions, a magnetic force of 1 mN is necessary to hold the MPM in discrete position. To obtain this holding force, the FPMs must be placed at a distance of 17 mm from the stop (d_1 in Figure 1).

TABLE I
DIMENSIONS AND REMANENT MAGNETIZATION OF PMS

Magnet	Dimensions (mm)	Remanent magnetization (T)
MPM	5 × 5 × 2	1.345
FPM	10 × 5 × 2	1.43

Figure 2 represents the three components of the total force exerted on the MPM (F_x, F_y and F_z) in function of its position along the x-axis. The different curves represent different driving current values (0 A, 3 A and 5 A) in the y-wire, called "x-axis switching wire". Here, the current in the x-wire (holding current) is zero. The discrete positions (–x, +y) and (+x, +y) are located at –0.5 mm and +0.5 mm respectively for a given stroke of 1 mm.

The component of the total force along the x-direction is represented in Figure 2a. When the MPM is in discrete position (±0.5 mm), a holding force of ±1 mN is exerted by the FPMs on the MPM. This force can be considered linear in function of the x-position because of the small stroke (1 mm) in comparison with the dimensions of the PMs (5 mm) and the long distance of the FPMs from the stop (d_1 = 17 mm in Fig. 1). If the FPMs are placed nearer to MPM or if the stroke is increased, non linearity would appear. The distance d_1 depends on the desired holding force (1 mN) and the remanent magnetization of the FPMs (1.43 T). When a current passes in the y-axis wire, the straight line is shifted upward. This upper shift corresponds to an addition of a positive electromagnetic force in comparison with the initial configuration. This force represents 3.9 mN and 6.5 mN for 3 A and 5 A driving currents respectively. The slope of the line for each driving current is not modified by the value of the driving current. Indeed, the slope which represents the gradient of the magnetic force applied to the MPM is only fixed by the position of the FPMs. This gradient is not affected by the driving current because the two effects, magnetic and electromagnetic, are independent.

The component of the total force along the y-direction is represented in Figure 2b. This force corresponds to the holding force. The scale accentuates the variation but it varies slightly in function of the x-position. The force value is a little bit higher for the 0 mm position (+0.43%) than for the ±0.5 mm position. Indeed, when the MPM is in the middle position (0 mm), the flux density generated by the FPMs around the MPM is maximum because the MPM and the two FPMs are aligned along the y-axis (Fig. 3b). For the two extreme positions (±0.5 mm), the flux density is a little lower because the MPM and the two FPMs are misaligned (Fig. 3a and 3c). The curves for different driving currents (0 A, 3 A and 5 A) are superimposed because the driving current has no effect on its value. The wire is indeed oriented along the y-axis.

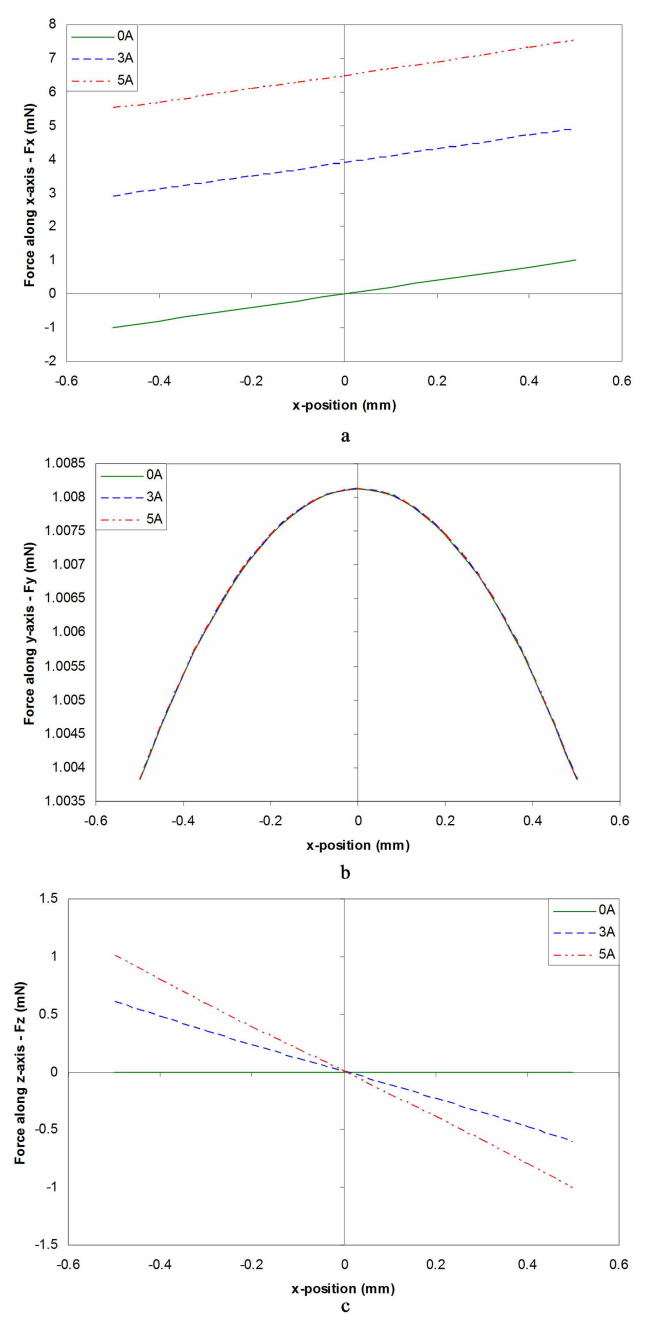

Fig. 2. Total force exerted on the MPM in function of its position and the driving current a. F_x b. F_y c. F_z

The F_z force corresponds to the vertical component of the total force (Fig. 2c) which is exerted when a current passes through a wire and when the MPM is misaligned with the driving wire (Fig. 3a and 3c). In this case, the orientation of the flux density around the wire is not totally along the z-axis but there is also a component along the x-axis which generates vertical force. It is null when the PM is in the 0 mm position and maximum when the PM is in discrete position (±0.5 mm) (Fig. 2c). Unlike the force along the x-axis, the slope of each line of the vertical force is function of the driving current. The vertical force is considered because it may disturb the functioning. Indeed, a vertical force can lift up the MPM if its value is higher than its weight.

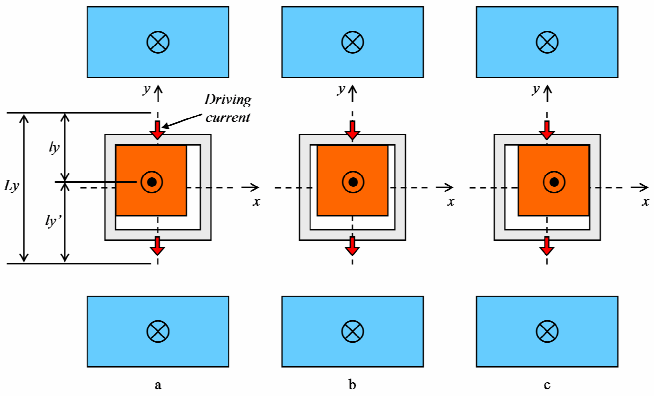

Fig. 3. Position of the MPM related to the FPMs
a. & c. misaligned b. aligned
Note: The two FPMs in the x-direction are not represented

In addition of these forces, when a driving current is used, a torque around the z-axis is exerted on the MPM when it is in discrete position. This torque is a function of two phenomena. The first one comes from the mismatch between the geometrical centre of the MPM and of the origin of the global coordinates system and the second one is due to the difference between ly and ly' in Figure 3a. However in the experiments, ly' – ly (1 mm) is very small in comparison with the length of the wire Ly (120 mm). Computations were done with semi-analytical computing software (RADIA) and it was found that this torque value is negligible (7×10^{-8} mN.mm with a 7 A driving current value) and does not disturb the trajectory of the MPM during a switch.

The second objective of this modelling is to compute the displacement of the MPM. In this case, the dynamic effects, the weight of the MPM, the friction and the adhesion are taken into account. A friction force ($F_{Friction}$) is computed with the weight (W) of the MPM and with the friction coefficient $\mu_{Friction}$, $F_{Friction} = W \times \mu_{Friction}$. The lateral friction generated by the holding effect which forces the MPM to be in contact with the lateral stop is also considered, $F_{Lat.\ Friction} = F_{Holding} \times \mu_{Lat.\ friction}$. These two friction forces ($F_{Friction}$ and $F_{Lat.\ friction}$) are subtracted from the total force exerted on the MPM along the displacement axis. For the adhesion phenomenon, an adhesion force ($F_{Adhesion}$) is computed with the weight (W) of the MPM and the adhesion coefficient $\mu_{Adhesion}$, $F_{Adhesion} = W \times \mu_{Adhesion}$. If the total force value enters in the range $[-F_{Adhesion}, +F_{Adhesion}]$ its value is set to zero. The three coefficients ($\mu_{Friction}$, $\mu_{Lat.\ friction}$ and $\mu_{Adhesion}$) were determined with experimental measurements using an inclined plane and with correlations using experimental displacement curves. The MPM is covered with a gold coating and is laterally in contact with a stop made up of aluminium and with glass on its lower face to avoid electrical contact between the MPM and the wires and to have a plane surface on which the MPM is moving. The values considered for the coefficients are: $\mu_{Friction}$ = 0.41 (gold – glass), $\mu_{Lat.\ friction}$ = 0.3 (gold – aluminium) and $\mu_{Adhesion}$ = 0.48 (gold – glass).

The previous Equations (1), (3) and (4) are implemented

directly in the displacement modelling. The total force exerted on the MPM is computed using these equations. The acceleration (γ) is computed in agreement with the Newton's inertial equation (5) and is function of the total force exerted on the MPM and of its mass (m = 449 ±1 mg). The values of velocity (v) and displacement (d) are computed by using time derivative of the acceleration. A MATLAB™ simulation is carried out by implementing this model.

$$\sum \vec{F} = m\vec{\gamma} = m\frac{d\vec{v}}{dt} = m\frac{d^2\vec{d}}{dt^2} \quad (5)$$

IV. Experimentation

A. Experimental actuator

An experimental device of a four discrete positions electromagnetic actuator was manufactured. The details of this experimental setup are given in Table II. The control signal is composed of two currents (driving and holding). A computer and a data acquisition board (PCI NI 6733) are used to generate two voltages using the Labview™ software. These two voltages are converted by two independent amplifiers (voltage-current converters), one for each axis. The input voltage and the output current of the amplifiers are respectively in the range [0 V, 10 V] and [0 A, 7 A]. The conversion is linear in this range and the bandwidth is 50 kHz.

TABLE II
DETAILS OF THE EXPERIMENTAL SETUP

Dimensions	
Overall dimensions	25 cm²
MPM dimensions	5 mm × 5 mm × 2 mm
FPMs dimensions	10 mm × 5 mm × 2 mm
Wire dimensions	Ø 0.5 mm × 120 mm
Thickness of the stop	3.5 mm
Height of the stop	2 mm
Thickness of the thin glass layer	160 µm
Distance d_1 (Figure 1)	17 mm
Distance d_2 (Figure 1)	410 µm
Materials	
PMs	NdFeB with gold coating
Stops	Aluminum
Wire	Copper
Remanent magnetization	
MPM	1.345 T
FPMs	1.43 T
Experimental parameters	
Theoretical stroke	1 mm
Controlling current range	0 A to 7 A

An electric pulse is used to switch between the discrete positions. During the experiments, the width of the pulse is always longer than the switching time in order to be sure that the MPM reaches the second discrete position before the end of the pulse. With this configuration, the MPM switches only between the discrete positions and can not reach another position. The holding force of this actuator is 1 mN when the MPM is in discrete position. When the MPM is near to the middle of the stroke (0 mm x-position), the holding force in the x-direction is near zero. If the electric pulse is shorter than the switching time, the friction and adhesion effects may stop the MPM in a position located between the two discrete positions. This actuator is then intrinsically not a bistable actuator but remains a digital actuator. However, the control is realized to obtain a bistable behaviour. Figure 4a represents an overall view of the experimental device. The MPM, the FPMs and the two wires are easily viewable in Figure 4b and the MPM on which a mirror is glued in Figure 4c.

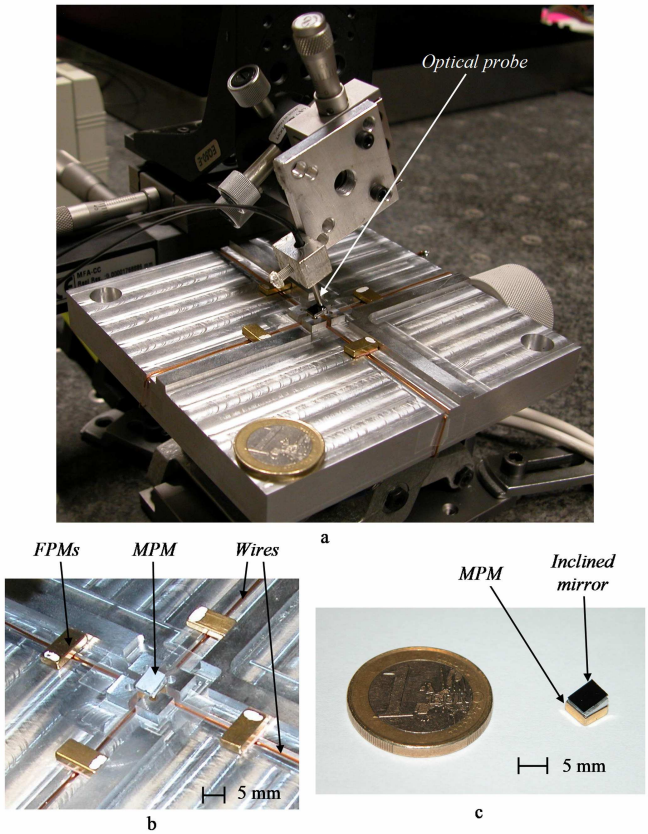

Fig. 4. a. Experimental device b. Zoom on the actuator c. MPM and mirror

B. Displacement sensor

During the experiments, a measurement of the displacement of the MPM was performed. This measurement is however not easy to realize because of the dimensions of the MPM and the stroke of the actuator. Moreover, the displacement measurement does not disturb the functioning of the actuator which does not need sensor when it is used in real applications. The choice of a miniature optical sensor was made because of the contact-less measurement technique (Fig. 4a). A mirror should be fixed on the MPM of the actuator (Fig. 4c). In normal conditions, the plane of the mirror should be orthogonal to the measurement axis which is collinear to the displacement axis. The principle of an inclined mirror is chosen in order to lower the position of the centre of gravity of the system "MPM + mirror" which avoids disturbances in the functioning of the actuator. In the configuration of the experimental measurements, the range of the sensor is 2 mm,

its resolution is 0.34 µm and the acquisition frequency is 500 Hz. The optical sensor is a fibre optic probe which is composed of an emission fibre and four reception fibres. Light coming from a LED is emitted by the emission fibre then reflected by the mirror and finally collected by the reception fibres. The output voltage of the sensor is a function of the quantity of light collected then of the distance between the sensor head and the mirror. The measurement technique using an inclined mirror has been described in details in [26].

C. *Experimental results*

Experimentations are realized with different driving current values [3 A, 7 A] and holding currents values [0 A, 5 A]. Figure 5 represents the evolution of the position of the MPM in the x-direction as function of time. Twelve switches between the +x and –x positions are shown. For this experiment, the y-axis wire is the driving wire and the x-axis wire is the holding wire. The driving current is +3 A or –3 A according to the displacement direction. The width of the current pulse is 125 ms and the MPM stays in discrete positions during 200 ms. The real stroke of the actuator is measured with the optical sensor, doing an average and taking into account the standard deviation on the twelve switches. The experimental stroke is (968.55 ± 0.23) µm. The difference between the experimental stroke (968.55 µm) and the theoretical one (1000.00 µm) can be explained by the real dimensions of the MPM (5.000 ± 0.006) mm and of the stop (5.944 ± 0.026) mm that are different from the theoretical dimensions due to manufacturing tolerances. The ± 0.23 µm value corresponds to repeatability of positioning of the actuator.

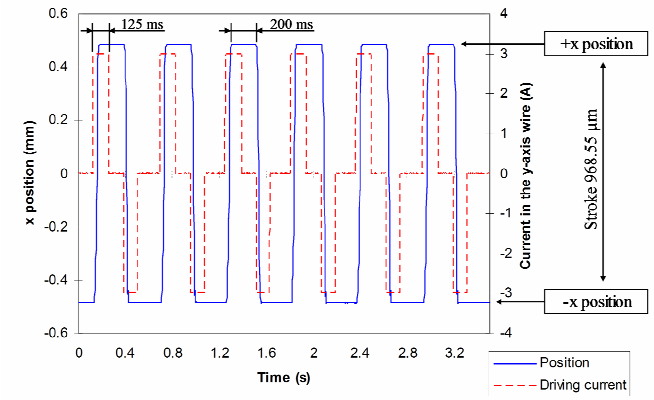

Fig. 5. Displacement curve in the x-direction – Twelve switches

Figure 6 represents five transitions between +x and –x positions. The values of the driving and holding currents are respectively 5 A and 0A. The values of the driving current do not permit to consider an instantaneous switch. There is then a transient effect between the discrete positions. At the beginning of the switch, the velocity is zero. Then, it increases to reach the maximum value when the MPM reaches the –x position. The increase of the velocity explains the shape of the displacement curve. It is observed that the transient effect between the two discrete positions is very repeatable: the curves of each switch are similar and are well superimposed. When the MPM reaches the –x position, an oscillation phenomenon is visible. This phenomenon corresponds to a measurement artefact of the optical sensor. Indeed, an orientation of the MPM modifies the quantity of light collected by the sensor which interprets the orientation by a modification of the position of the MPM.

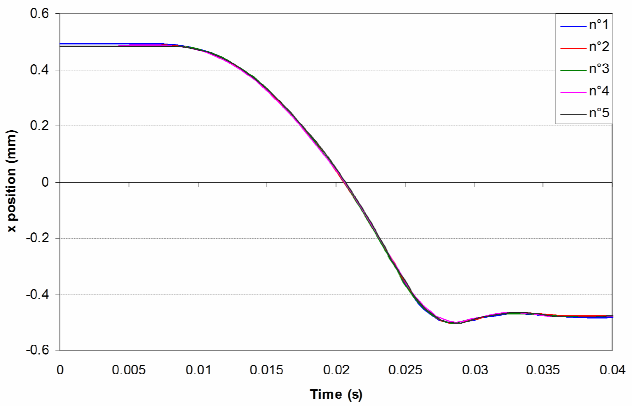

Fig. 6. Five switches from the +x position to the –x position

The next results emphasize the influence of the driving and holding currents on the switch between two discrete positions. Figure 7a represents the evolution of the transient effect when the driving current increases from 3 A to 7 A without holding current. For these current values, the switching time ranges from 12.1 ms to 29.1 ms. It is observed that the switching time decreases when the driving current increases. In this case, the actuation force increases too, then the switching time is reduced. Figure 7b represents the evolution of the transient effect with a 5 A driving current value and when the holding current increases from 0 A to 5 A. For these currents values, the switching time ranges from 15.7 ms to 22.9 ms. The switching time increases when the holding current rises because of the increase of the lateral friction generated by the holding current.

D. *Comparison between experimental and simulated dynamic behaviour*

The displacement modelling previously presented was used for the comparison with the experimental results. With this modelling, the displacements were computed for any driving and holding currents. The comparison for driving currents from 3 A to 7 A without holding current (Fig. 7a) shows a very good correlation between experimentation and simulation results. The shape of the displacement curves and the switching times are very similar in each configuration. The oscillation phenomenon generated by the artefact of measurement is visible on each experimental curve but not on the modelled curve because this was not taken into account in the modelling.

Figure 7b represents the comparison between experimentation and simulation for 5 A driving current with 0 A, 1 A, 3 A and 5 A holding current respectively. The correlation between experimentation and simulation is still

good whatever the holding current value which means that the lateral friction integrated in the modelling corresponds to the experimental behaviour observed. As it is mentioned before, the holding current may be used to reduce the straightness error of the actuator during a switch. When a holding current is used, an increase of the holding effect forces the MPM to be in contact with the lateral stop. Moreover, if exterior disturbances can potentially disturb the switch of the MPM, the holding current, which forces the MPM to be in contact with the stop, can be adapted in order to reduce the straightness error due to the disturbance. One of the prospects is to improve the measurement of the lateral displacement during a switch to get the experimental value of the straightness error.

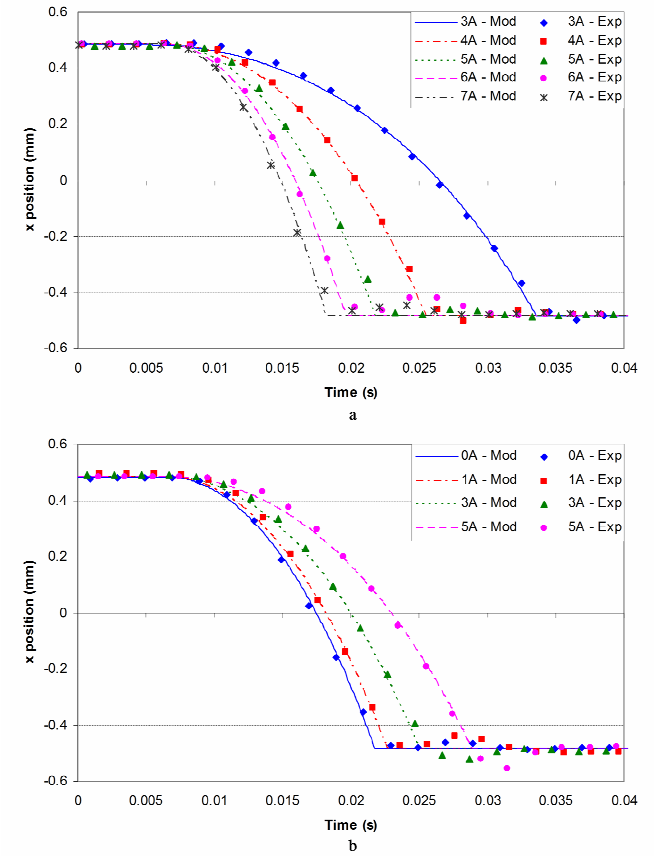

Fig. 7. Comparison between simulation and experimentation
a. Influence of the driving current b. Influence of the holding current

On the experimental displacement curves, the switching times are not easy to be determined because of the oscillation phenomenon observed when the MPM reaches the target position. To compare simulation and experimentation, the rise times are then studied. The rise time corresponds to the time necessary to pass from 10% to 90% of the total stroke of the MPM. In Figures 8a and 8b, the same experimental points are plotted in two different ways in order to highlight the influence respectively of the driving and holding current on the rise time. The dots represent the experimental values and the modelled results are represented by the lines. In Figure 8a, the different lines correspond to different holding current values from 0 A to 5 A. In Figure 8b, the lines correspond to different driving current values from 3 A to 7 A.

In Figure 8a, when the holding current increases, the rise time and the lowest driving current necessary to switch increase. Indeed, without holding current, 3 A driving current is enough to switch the MPM but with 3 A holding current, the former driving current is no more sufficient. In this configuration, the MPM doesn't switch because of the high lateral friction which is higher than the driving force. In Figure 8b, the influence of the driving and holding currents previously described are also observed. Besides, the increase in the rise times generated by the holding current is more important on low driving currents than on high driving currents. The total force exerted on the MPM corresponds to the driving force minus the friction and lateral friction forces with the consideration of the adhesion effect. When a low driving current is used, the total force is slightly higher than zero. The MPM switches then slowly. When a holding current is added, the lateral friction is increased. This increase represents a high variation of the total force then of the rise time (4.1 $ms \cdot A^{-1}$ with 3 A driving current). On the opposite side, when a high driving current is used, the total force is clearly higher than zero. The MPM switches then quickly. In this case, when a holding current is added, the increase of the holding force represents a small variation of the total force then a small variation of the rise time too (0.3 $ms \cdot A^{-1}$ with 7 A driving current).

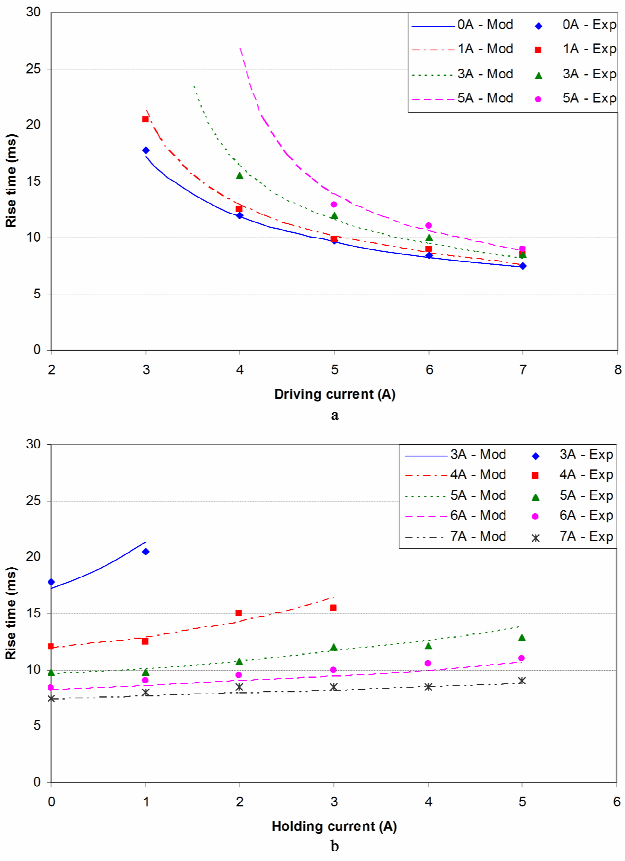

Fig. 8. Comparison between the experimental and modelled rise times
a. Influence of the driving current b. Influence of the holding current

Figures 7 and 8 show that the displacement curves and the rise times computed using the modelling correspond well to the experimental measurements for all the range of driving and holding currents. The average relative error between experimental and modelled rise times (Fig. 8) represents 3.6%. From this accordance between experimental and simulated results, it is considered that the mechanical and magnetic hypotheses realized in the modelling are suitable and that the phenomena considered in the modelling are really those which characterize the actuator behaviour.

Finally, the measurement of the payload capability was realized. On the upper side of the MPM, a mass was fixed (the mirror was removed) and the set "MPM + mass" was switched. The maximum mass displaced experimentally by the actuator was 1.3 g with a 6.5 A driving current without holding current.

V. Comparisons of performances

Table III gives a comparison of the performances between the presented actuator and other digital actuators. The dimensions, degree of freedom, energy consumption for a switch, switching time, stroke and driving force are compared. It is observe that the dimensions of the presented actuator are greater than the other actuators. Most of them have been indeed manufactured using microfabrication. However, this big size permits to have a longer stroke and to produce higher driving force. The energy consumption to switch is among the highest because of the big size. The switching time is about the same among the different actuators and represents several milliseconds except for one actuator which is lower than a millisecond. Finally, the main advantage of the presented actuator is the two degrees of freedom which permits to move the MPM independently in two orthogonal directions.

VI. Conclusion

Based on digital principle, an electromagnetic actuator having four discrete positions was developed. A modelling of this actuator was realized using the charge model. An experimental actuator was designed using this modelling and manufactured. Experimentations were realized and the displacement of the MPM was measured using an optical sensor. The displacement curves and the rise times were compared to the simulated results. A good correlation between the numerical and experimental results was observed for all the range of controlling (driving and holding) currents which means that the phenomena considered in the modelling are really those which control the actuator behaviour. In this work, only one axis of the actuator was presented because the objective was to validate the principle of discrete displacement. In a future work, the two axes of displacement will be presented.

During the actuator manufacturing, the wires and the thin glass layer were manually assembled. This step is very important because the performances of the actuator strongly depend on it. In near future, the influence of the assembly and manufacturing errors (error in the positioning or orientation of the FPMS and wires, variation of the remanent magnetization of the PMs, etc.) will be studied and a second four discrete positions actuator will be designed and manufactured considering this analysis. In addition, the straightness of displacement will be studied and the influence of the driving and holding currents on it will be quantified.

Applications can be found as well with single actuator devices as multiple actuators devices and will be investigated in future works. For example, 2D micro tribometers with single actuator device is a new way to analyze contact between two bodies. Another application using a multiple actuators device can be applied to the optical profilometry field to get new long-range instruments including 2D positioning stage composed of numbers of microfabricated elementary digital electromagnetic actuators. In this case, the actuation force of this stage will be the sum of the whole elementary forces and this device will have two orthogonal displacement axes, like each elementary digital actuator.

References

[1] J. Gu, "Development of 6 DOF magnetically levitated instrument with nanometre precision", Dpt Mechanical Engineering, Thesis, Texas, A&M university, Texas, USA, 2003.

[2] T. Hu, W.-J. Kim, "Extended range six-DOF high precision positioner for wafer processing", *IEEE/ASME Transactions on Mechatronics*, vol. 11, no 6, pp. 682-689, 2006.

[3] H. Kube, V. Zoeppig, R. Hermann, A. Hoffmann and E. Kallenbach, "Electromagnetic miniactuators using thin magnetic layers", *Smart Mater. Struct.*, vol. 9, pp. 336–341, 2000.

[4] L. Lu, Z. Chen, B. Yao, "Desired compensation adaptive robust control of a linear-motor-driven precision industrial gantry with improved cogging force compensation", *IEEE/ASME Transactions on Mechatronics*, vol. 13, no 6, pp. 617-624, 2008.

[5] P. Karutz, T. Nussbaumer, W. Gruber, J.W. Kolar, "Novel magnetically levitated two-level motor", *IEEE/ASME Transactions on Mechatronics*, vol. 13, no 6, pp. 658-668, 2008.

[6] L. Yan, I.-M. Chen, C. K. Lim, W. Lin, K.-M. Lee, "Design and analysis of a permanent magnet spherical actuator", *IEEE/ASME Transactions on Mechatronics*, vol. 13, no 2, pp. 239-248, 2008.

[7] H. Son, K.-M. Lee, "Distributed models for design and control of PM actuators and sensors", *IEEE/ASME Transactions on Mechatronics*, vol. 13, no 2, pp. 228-238, 2008.

[8] O. Cugat, *Micro-actionneurs électromagnétiques MAGMAS*, Hermès science publications, Paris, 2002, p. 340.

TABLE III
Comparison of performances of digital actuators

Actuator	Dimensions	Degree of Freedom	Energy consumpt.	Switching time	Stroke	Driving force
Matsuura *et al* [9]	2.4 cm²	1	0.2 mJ	20 ms	90 µm	/
Fu *et al* [10]	1.6 cm²	1	58 mJ	10 ms	50 µm	0.07 mN
Bintoro *et al* [11]	0.02 cm²	1	1.24 mJ	2 ms	71 µm	1.65 mN
Chen *et al* [21]	0.0003 cm²	1	/	5 ms	100 µm	1 mN
Dieppedale *et al* [24]	0.00004 cm²	1	0.048 mJ	0.03 ms	≈ 10 µm	/
Presented work	25 cm²	2	57 mJ	12.1 ms – 29.1 ms	969 µm	> 9mN

[9] T. Matsuura et al., "Silicon micro optical switching device with an electromagnetically operated cantilever", *Sensors and Actuators*, 83, pp. 220-224, 2000.
[10] S. Fu, G. Ding, H. Wang, Z. Yang, J. Feng, "Design and fabrication of a magnetic bi-digital electromagnetic MEMS relay", *Microelectronics Journal*, vol. 38, pp. 556-563, 2007.
[11] J.S. Bintoro, A.D. Papania, Y.H. Berthelot, P.J. Hesketh, "Bidirectional electromagnetic microactuator with microcoil fabricated on a single wafer: static characteristics of membrane displacements", *J. Micromech. Microeng.*, vol. 15, pp. 1378-1388, 2005.
[12] R. Luharuka, P.J. Hesketh, "A bistable electromagnetically actuated rotary gate microvalve", *J. Micromech. Microeng.*, 18, 2008.
[13] A. Bowles, A. Rahman, T. Jarman, P. Morris, J. Gore, "Bistable electromagnetic actuators for tactile displays", *ACTUATOR 2006, 10th International Conference on New Actuators,* Bremen, Germany, pp. 816-819, June 14-16, 2006.
[14] M. Hafez, M. D. Lichter, S. Dubowsky, "Optimized binary modular reconfigurable robotic devices", *IEEE/ASME Transactions on Mechatronics*, vol. 8, pp. 18-25, 2003.
[15] B. D. Jensen, M. B. Parkinson, K. Kurabayashi, L. L. Howell, M. S. Baker, "Design optimization of a fully-compliant bistable micro-mechanism", *Proceedings of 2001 ASME International Mechanical Engineering Congress and Exposition*, New-York, USA, Nov. 11-16, 2001.
[16] P. Fang, F. Ding, Q. Li, "Novel high-response electromagnetic actuator for electronic engraving system", *IEEE Transactions on Magnetics*, vol. 42, no 3, 2006.
[17] Q. Li, F. Ding, C. Wang, "Novel bidirectional linear actuator for electrohydraulic valves", *IEEE Transactions on Magnetics*, vol. 41, no 6, 2005.
[18] B. Liu, D. Li, X. Yang, X. Li, "Design and Fabrication of a Micro Electromagnetic Actuator", *1st IEEE International Conference on Nano/Micro Engineered and Molecular Systems (NEMS 2006),* Zhuhai, China, Jan. 18-21, pp. 353-356, 2006.
[19] B. Liu, D. Li, "Design and fabrication of a micro electromagnetic relay", *Proceedings of the 2006 IEEE International Conference on Mechatronics and Automation*, Luoyang, China, June 25-28, 2006.
[20] K.R. Cochran, L. Fan, D.L. DeVoe, "High-power optical microswitch based on direct fiber actuation", *Sensors and Actuators*, A 119, pp. 512-519, 2005.
[21] W.C. Chen, C. Lee, C.Y. Wu, W. Fang, "A new latched 2 × 2 optical switch using bi-directional movable electrothermal H-beam actuators", *Sensors and Actuators,* A 123-124, pp. 563-569, 2005.
[22] M. Freudenreich, U. Mescheder, G. Somogyi, "Simulation and realization of a novel micromechanical bi-digital switch", *Sensors and Actuators*, A 114, pp. 451-459, 2004.
[23] F. Pieri, M. Piotto, "A micromachined bistable 1×2 switch for optical fibers", *Microelectronic Engineering*, 53, pp. 561-564, 2000.
[24] C. Dieppedale et al., "Magnetic digital micro-actuator with integrated permanent magnets", *Sensors, Proceedings of IEEE*, Vienne, Austria, pp. 4, Oct. 24-27, 2004.
[25] E.P. Furlani, *Permanent magnet and electromechanical devices – Materials, analysis and applications*, Academic Press, San Diego, 2001, p. 518.
[26] C. Prelle, F. Lamarque, P. Revel, "Reflective optical sensor for long-range and high-resolution displacements", *Sensors and Actuators*, A 127, pp. 139-146, 2006.

Laurent Petit received the M.S. degree from l'Université de Technologie de Compiègne (France) in 2006. He is currently working toward the Ph.D. degree in mechanical engineering.
His current interest includes digital devices, electromagnetic actuation, and miniature actuators.

Christine Prelle received the DEA degree in automatic control from l'Université Claude Bernard Lyon 1 (France) in 1994 and the Ph.D. degree in industrial automatic control from l'INSA Lyon (France) in 1997.
Since 1998, she is Associate professor in control engineering at l'Université de Technologie de Compiègne. Her research includes micromechatronics and control.

Emmanuel Doré received the Ph.D. degree in bio-mechanical design from l'Université de Technologie de Compiègne in 1999.
He is actually Associate professor in mechanical systems at l'Université de Technologie de Compiègne. His research includes mechanical design and multiphysics modelling.

Frédéric Lamarque received the DEA degree in electronics in 1994 and the Ph.D. in electronics in 1998 from l'Université Paris Sud Orsay (France).
Since 2000, he is Associate professor in sensors and instrumentation at l'Université de Technologie de Compiègne. His research includes microsensors and microactuators technologies.

Maxence Bigerelle received the Ph.D. degree in Mechanic and Material Sciences in 1999.
He is Professor in materials science, Engineer in Computer Sciences, Medical Expert in Biomaterials at the University Hospital Centre of Lille (France) and Capacitation of Research Directorship in Physical Sciences (2002). His research includes Surfaces and Interfaces morphological characterisation, Multi-scale Modelling, Fractal & Chaos, Biomaterials and Nanostructures.
Actually, he is Director Assistant of the Materials Research Group in the Laboratory Roberval.